Report

Cell Reports

State-Dependent Subnetworks of Parvalbumin-Expressing Interneurons in Neocortex

Graphical Abstract

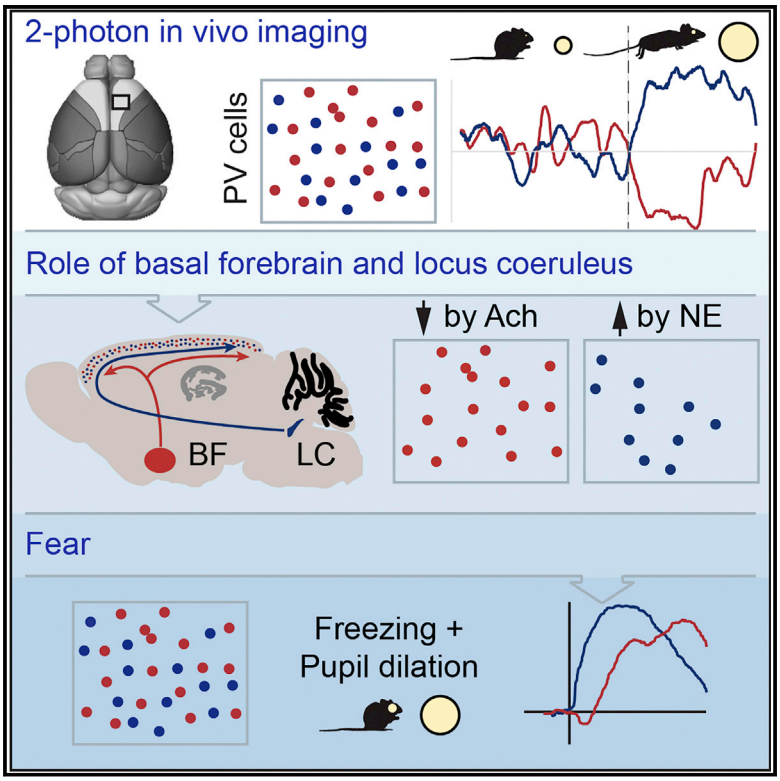

Authors

Pablo Garcia-Junco-Clemente, Elaine Tring, Dario L. Ringach, Joshua T. Trachtenberg

Correspondence

pgarciajunco@gmail.com

In Brief

Fast-spiking interneurons in cortex are generally viewed as functionally homogeneous. Garcia-Junco-Clemente et al. present evidence that across diverse cortical areas there are at least two functionally distinct subnetworks of these interneurons, which can be independently engaged as a function of behavior.

Highlights

- Fast-spiking interneurons in cortex establish functionally distinct sub-networks
- These subnetworks are stable and independent
- They appear to be differentially engaged by basal forebrain and *locus coeruleus*
- These sub-networks are differentially recruited by diverse behaviors

Garcia-Junco-Clemente et al., 2019, Cell Reports *26*, 2282–2288
February 26, 2019
https://doi.org/10.1016/j.celrep.2019.02.005

CellPress

OPEN ACCESS
CellPress

Cell Reports
Report

State-Dependent Subnetworks of Parvalbumin-Expressing Interneurons in Neocortex

Pablo Garcia-Junco-Clemente,[1,2,4,*] Elaine Tring,[1] Dario L. Ringach,[1,3] and Joshua T. Trachtenberg[1]
[1]Department of Neurobiology, David Geffen School of Medicine at UCLA, Los Angeles, CA 90095, USA
[2]Instituto de Biomedicina de Sevilla, IBiS, Hospital Universitario Virgen del Rocío/CSIC/Universidad de Sevilla and Departamento de Fisiología Médica y Biofísica, Universidad de Sevilla, and CIBERNED, Seville, Spain
[3]Department of Psychology, University of California, Los Angeles, Los Angeles, CA 90095, USA
[4]Lead Contact
*Correspondence: pgarciajunco@gmail.com
https://doi.org/10.1016/j.celrep.2019.02.005

SUMMARY

Brain state determines patterns of spiking output that underlie behavior. In neocortex, brain state is reflected in the spontaneous activity of the network, which is regulated in part by neuromodulatory input from the brain stem and by local inhibition. We find that fast-spiking, parvalbumin-expressing inhibitory neurons, which exert state-dependent control of network gain and spike patterns, cluster into two stable and functionally distinct subnetworks that are differentially engaged by ascending neuromodulation. One group is excited as a function of increased arousal state; this excitation is driven in part by the increase in cortical norepinephrine that occurs when the *locus coeruleus* is active. A second group is suppressed during movement when acetylcholine is released into the cortex via projections from the *nucleus basalis*. These data establish the presence of functionally independent subnetworks of Parvalbumin (PV) cells in the upper layers of the neocortex that are differentially engaged by the ascending reticular activating system.

INTRODUCTION

Cortical state—the pattern of spontaneous activity controlled by neuromodulatory input from the ascending reticular activating system and by local inhibition—determines the pattern of network spiking in response to sensory stimuli (Harris and Thiele, 2011; Stringer et al., 2018; Musall et al., 2018). Roughly half of the local inhibitory neurons in the cortex are parvalbumin-expressing, fast-spiking "basket" cells, often referred to simply as Parvalbumin (PV) cells. These interneurons regulate network gamma oscillations and control the gain of local pyramidal cell networks (Polack et al., 2013; Wilson et al., 2012; Lee et al., 2012). The firing rates of PV cells reflect the behavioral state, and their activities are modulated by acetylcholine (Alitto and Dan, 2013) and likely by norepinephrine, both of which are released into the cortex by ascending projections from the *nucleus basalis* of the basal forebrain and the *locus coeruleus*, respectively. This interaction between the reticular activating system and cortical PV cells is poorly understood.

To investigate this interaction, we used resonant scanning 2-photon calcium imaging to monitor the spontaneous activity of PV cells in alert head-fixed mice and combined this approach with behavioral, pharmacological, and optogenetic manipulations that engage or suppress neuromodulation. Given the dominant role of brain state on sensory responses and sensory-guided decision-making in the cortex (Musall et al., 2018), we focused our efforts on a region of the secondary motor cortex often referred to as the anterior lateral motor cortex, a region strongly engaged during decision-making (Guo et al., 2014, 2017; Inagaki et al., 2018) as well as the primary visual cortex (V1).

RESULTS

To specifically label and track the activities of PV neurons in the anterior lateral motor cortex (ALM) and primary visual cortex, an adeno-associated virus containing a flexed construct of the genetically encoded calcium indicator GCaMP6s (Chen et al., 2013) was injected into either region in mice from a PV-IRES-Cre driver line (Hippenmeyer et al., 2005) that had previously been crossed with the Ai9 line of mice containing a flexed red fluorescent protein, tdTomato (Madisen et al., 2010; Figure 1A). Thus, all PV cells in the cortex expressed tdTomato, whereas only PV cells in the vicinity of the virus injection also expressed GCaMP6s. Fluorescent changes in GCaMP6s were imaged at 15.5 frames per second using a custom-built resonant scanning 2-photon microscope. Pupil diameter and locomotive state were simultaneously tracked using dedicated cameras because their fluctuations track shifts in the cortical state that are associated with changes in adrenergic and cholinergic activity (Reimer et al., 2014, 2016; McGinley et al., 2015).

Two Functionally Defined Groups of PV Cells

We first examined responses in the ALM. In each imaged mouse, we qualitatively observed two groups of responses. During epochs when mice were running and the pupils were dilated, one group was clearly active, whereas the other group was

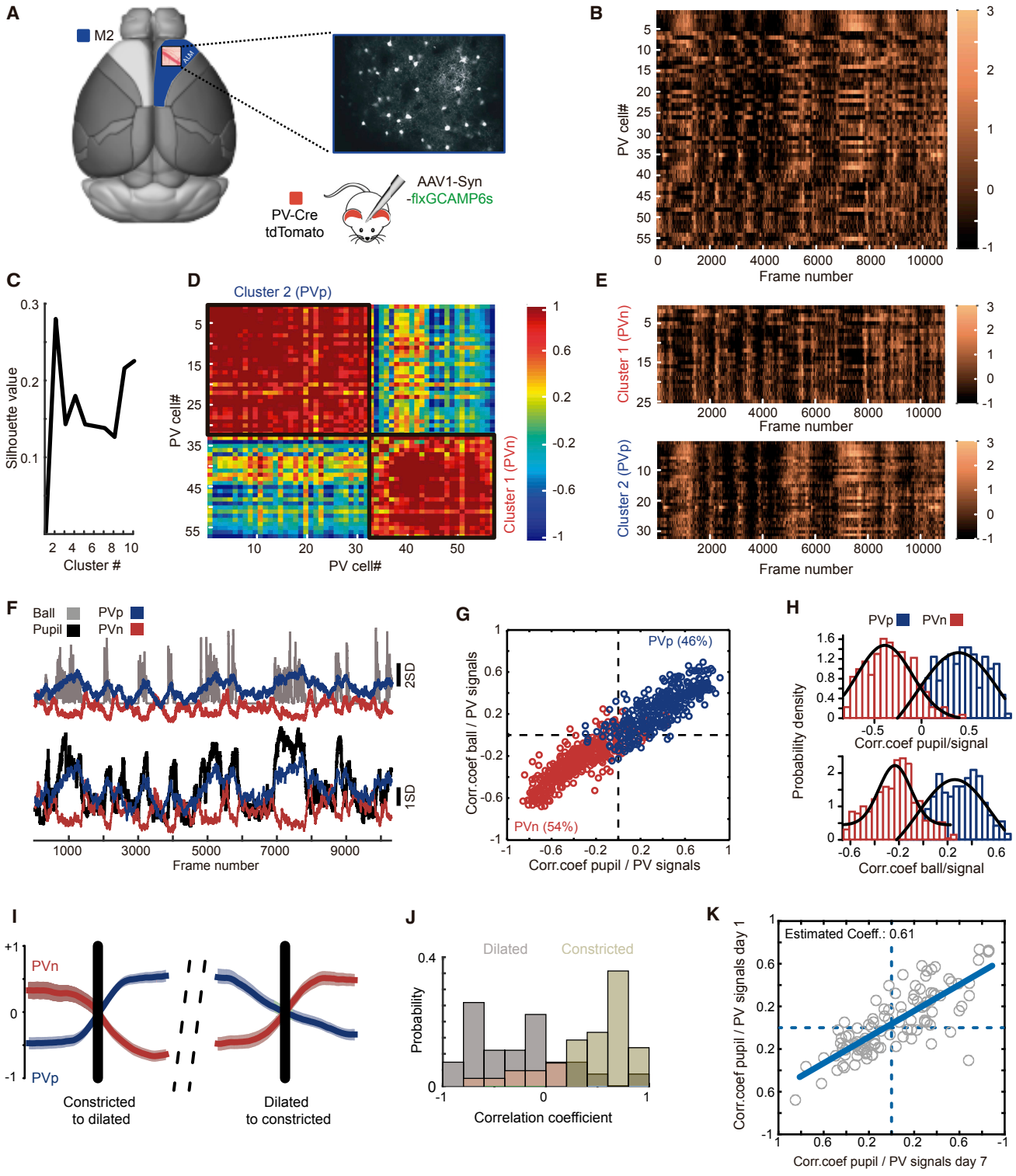

Figure 1. Two Functional Groups of PV Cells in the ALM

(A) Schematic of a mouse brain, highlighting area M2 and identifying the craniotomy location. On the right is an example of GCaMP6s expression in PV cells taken through the imaging window.

(B) An example of GCaMP6s fluorescence changes imaged across 57 PV cells over approximately 11,000 frames (roughly 12 min) in an alert, head-fixed mouse. The colored scale bar on the right is in units of *Z* score.

(legend continued on next page)

suppressed (Figure 1B). The presence of two functional groupings was confirmed by *post hoc* cluster analysis of the correlation coefficients for all PV cells in each field of view (Figures 1C–1E). When we measured the temporal correlation coefficient between GCaMP6s signals of the PV cells in each of these two groups with measures of pupil diameter and, separately, locomotion, we found that PV cells in one cluster were almost always positively correlated with locomotion and pupil dilation, whereas the activities of cells in the other cluster were almost always negatively correlated with these two measures (Figures 1F–1H). Although there was variability from animal to animal and from one imaging plane to another, the numbers of PV cells in each of these two groups was roughly equal across all animals and imaging planes. To simplify, hereafter we will refer to cells whose activities are positively correlated with locomotion and pupil diameter as PVp cells and to cells whose activities are negatively correlated with these measures as PVn cells. PVn cells were typically more active than PVp cells during quiescence, but the transition to running drove their suppression with concomitant elevation of PVp responses (Figure 1I). Notably, although the activities of these two functional clusters were negatively correlated during locomotion, they were highly synchronous during periods of rest (Figure 1J), indicative of a common excitatory input. To examine whether cells in each of the groups remained faithful in their responses over time, we repeatedly imaged the same cells over an interval of 1 week and plotted their correlation coefficients to pupil diameter and locomotion at both time points. Cells that were positively or negatively correlated with locomotion and pupil dilation at the first time point remained so 1 week later (Figure 1K), indicating that these are functionally stable subgroups. Two functional clusters were also found in the primary visual cortex, although the ratios were unequal at this posterior cortical region, with roughly two-thirds of PV cells positively correlated with an increased arousal state (Figure S1). To determine whether PVp and PVn cells establish spatial clusters, we examined the covariance of each imaged neuron's response to all other imaged neurons in each imaging plane as a function of distance. We found no relationship between correlated responses and distance, indicating that neighboring PV cells do not necessarily have similar responses (Figure S2).

Cholinergic Modulation of One Group of PV Cells

When mice transition from quiet wakefulness to running, there is a concomitant increase in pupil diameter as the arousal state increases, and these differentially affect cortical activity (Vinck et al., 2015). This state change engages the cholinergic *nucleus basalis* of the basal forebrain as well as the adrenergic nucleus of the *locus coeruleus* (Reimer et al., 2016). Cortical projections from these nuclei release acetylcholine and norepinephrine, respectively, into the cortex, which then act to modulate neural responses (Foote et al., 1980; Polack et al., 2013; Bennett et al., 2014; Lee et al., 2014). To examine whether PVp and PVn cells respond differently to acetylcholine or norepinephrine, we undertook a series of experiments in which we imaged PV cell responses while simultaneously manipulating cholinergic and adrenergic signaling.

To examine the influence of acetylcholine on PV cell responses, we imaged PV cells before and after local pharmacological blockade of both muscarinic and nicotinic cholinergic receptors via atropine and mecamylamine, respectively. The concentrations of these agents were chosen from previously published studies of cortical activity *in vivo* (Polack et al., 2013). Blockade of cholinergic signaling altered the activities of previously identified PVn cells; the correlation coefficients of their activities with locomotion and pupil diameter, which had been negative, now all shifted toward 0 because the activities of these PV cells were no longer modulated by the cholinergic release that occurs when mice run (Figure 2). By contrast, the coefficients of PVp cells to locomotion and pupil diameter were not significantly affected. We examined the possibility of optogenetically stimulating the basal forebrain while imaging PV responses in the ALM but could find no way of positioning the objective lens over the ALM while also simultaneously securing a fiberoptic cannula to the skull that would be appropriately positioned to target the basal forebrain. The ALM and basal forebrain are too close along the rostral-caudal axis to permit this.

PV Cell Responses to Stimulation of the *Locus Coeruleus*

Pharmacological blockade of adrenergic receptors in the ALM via local injection of the $\alpha 1$, $\alpha 2$, and β noradrenergic receptor antagonists yohimbine and propranolol silenced cortical activity,

(C) Plot of silhouette value versus cluster number following k-means cluster analysis, identifying 2 major functional clusters of PV cells.
(D) Plot of the correlation coefficient of the activity of each cell in (B) to all other cells. Note the emergence of two groups, labeled cluster 1 and cluster 2. The scale bar on the right is units of correlation coefficient.
(E) Time series of GCaMP6 responses for cells in cluster 1 in (D), bottom right, and cluster 2 in (D), top left. Note the negative correlation in the responses of these two groups. The heatmap scale bar is as in (B).
(F) Plots of the mean time series of cluster 1 and cluster 2 in (E) (red trace and blue trace, respectively) to the *Z*-scored time series of running speed (ball, top, gray trace) and pupil diameter (pupil, bottom, black trace). Note the strong positive and negative correlations between mean PV cell responses for each cluster and locomotion and pupil diameter.
(G) Plot of each cell's correlation coefficient to pupil diameter (abscissa) and to locomotion (ordinate). Cells colored blue were positively correlated with each other, as were cells colored red. 11 mice, 21 fields of view, 747 PV cells (344 PVp, 403 PVn).
(H) Distributions of the correlation coefficients for the cells plotted in (G). Hartigan's dip test for unimodality, $p = 0.02$, indicates that the distribution is not unimodal.
(I) Example traces of mean PVp (blue) and PVn (red) GCaMP6 responses at the transition to running (left) when the pupil diameter dilates and the transition from running to stopping (right), when the pupil diameter constricts. The black line indicates the transition time. Values are *Z* scores.
(J) Histograms showing the distributions of correlation coefficients between PVp and PVn time series for individual epochs of pupil dilation or constriction. Note that PVp and PVn groups are strongly correlated (values greater than 0.5) when the pupil is constricted (beige bars). When the pupil is dilated (gray bars), coefficients drop below 0, indicating that these two groups of cells are now negatively correlated.
(K) Plot of the correlation coefficient between each imaged PV cell's response and pupil diameter, measured one week apart. 105 PV cells were longitudinally imaged in 7 mice. Correlation coefficient = 0.79, R-square of the linear regression = 0.63, slope = 0.61, $p < 0.001$.

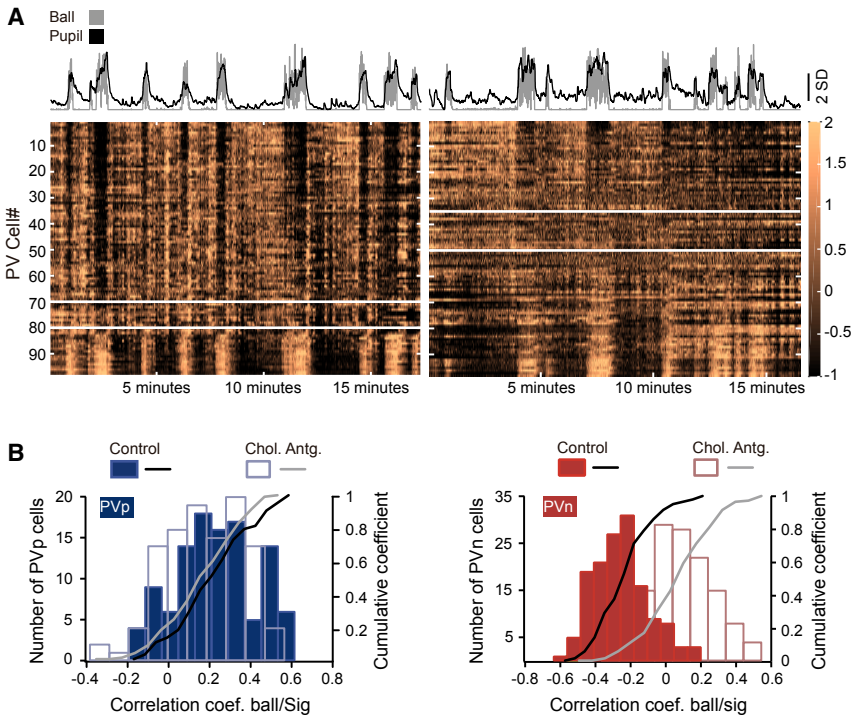

Figure 2. PVn Cells Are Suppressed by Acetylcholine

(A) Example time series of GCaMP6s responses for the same PV cells before (left) and after (right) intracortical injection of atropine and mecamylamine. Plotted above each is the time series plot of pupil diameter (black) and ball motion (gray). In each GCaMP6s time series, cells that are negatively correlated with pupil diameter and running are above the top white horizontal line, whereas those that are positively correlated are below the bottom white line. Activities of cells between these two lines are not significantly correlated with either pupil diameter or running speed (Spearman's Rho). Note that, after cholinergic blockade, the number of PVn cells (those above the topmost white line) is roughly half of what it was prior to blockade.

(B) Left: histogram and cumulative distributions of response coefficients to pupil diameter of 143 PVp cells imaged before cholinergic blockade and for these same cells after blockade. Note the absence of an effect of blockade on their coefficients. n = 3 mice; p = 0.39, Kolmogorov-Smirnov test. Right: the same plots but for PVn cells. 109 cells were imaged in the same 3 mice. Note the shift in coefficients toward 0. $p < 0.001$, Kolmogorov-Smirnov test.

rendering this approach ineffective as a means to interrogate the effect of norepinephrine on PV cell responses. We note that similar cortical silencing with adrenergic blockade has also been reported for pyramidal neurons in the primary visual cortex (Polack et al., 2013).

The *locus coeruleus* is located approximately 8.25 mm caudal to the ALM. This large berth made it possible to place a fiberoptic cannula into the *locus coeruleus* (LC), to cement this cannula to the skull with an attached fiber patch cord, and to position the objective lens over the ALM without interference. Using this approach, we recorded the activity of PV cells while optogenetically stimulating the LC using trains of 40 10-ms light pulses delivered at the imaging frame rate (15.5 per second). Experiments were conducted in double transgenic offspring from crosses of PV-Cre and Th-Cre driver line mice. An adeno-associated virus containing a flexed channelrhodopsin-2 tagged to tdTomato was injected into the LC based on stereotaxic coordinates (Figure 3A). Notably, because we could only genotype based on Cre expression, we could not know *a priori* whether the mice expressed Cre recombinase only in the LC, only in PV cells, or both. Expression in the LC was confirmed by *post hoc* examination of brain sections to determine whether tdTomato and, thus, ChR2 was or was not expressed (Figure 3B). Mice were assigned to experimental or control groups based on these results, with control mice lacking tdTomato and ChR2 expression in the LC. As above, GCaMP6s expression in PV cells was achieved and verified using virus-mediated delivery of flexed GCaMP6s.

PV cell activity was recorded for 20 min, and during this time, 18–20 epochs of blue light trains were delivered to the LC. In mice lacking ChR2 expression in the LC, blue light flashes had a small effect on measures of pupil diameter and PVp responses (Figure 3C). In experimental mice, which did express ChR2 in the LC, blue light flashes were followed by large pupil dilation, a known effect of LC stimulation (Reimer et al., 2016), and PVp cells experienced an equally large increase in relative GCaMP6s signal (Figure 3D). PVn cell responses, by contrast, were not significantly changed. Interestingly, in some trials, LC stimulation not only drove an increase in pupil diameter, but it also drove changes in motor state; the tail would go up and the mouse would begin to walk or run on the treadmill. These trials were not included in our analysis because the cholinergic modulation associated with the motor movement would impair our analysis.

PV Cell Responses during Associative Fear

We wondered whether these neuromodulatory effects would also be manifested during behavior. Associative fear is a useful behavior for such an examination because, in mice, fear is characterized by motor freezing and pupil dilation, and, thus, the responses of PVp and PVn cells should track accordingly.

To examine this, the same cohort of PV cells was longitudinally imaged before and after mice learned an associative fear-conditioning paradigm in which exposure to a 2-kHz tone for 15 s was paired with a 1-s-long foot shock during the final second of the tone (Figure 4A). Learning was measured behaviorally by tracking freezing in response to the tone and by measures of pupil diameter and running (Figure 4B).

In these experiments, the learned association between tone and foot shock was clear. Prior to exposure to the tone and foot shock association, mice showed no behavioral response to tones; neither pupil dilation nor running speed were altered

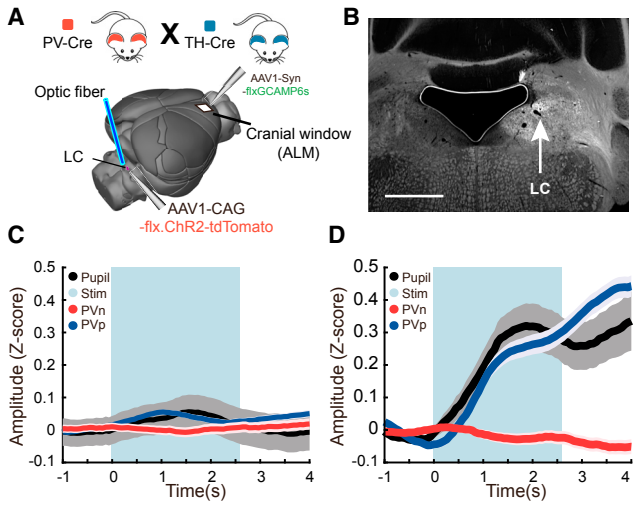

Figure 3. Direct Optogenetic Stimulation of the LC

(A) Schematic showing the placement of a fiberoptic cannula into the brain to stimulate the LC as well as the position of the imaging window in the ALM.

(B) An example image showing the fluorescence of tdTomato-tagged Channelrhodopsin-2 following adeno-associated virus (AAV) delivery of a flexed construct into Th-Cre mice. Because ChR2 is membrane-bound, the LC and its axonal projections are labeled. The location of the cell bodies in the LC is shown by the arrow. The black region to the left is an air bubble over the ventricle. The tissue above and to the right of this is the cerebellum. Scale bar, 1 mm.

(C) Control mice; time series measures of pupil diameter and PVp and PVn cells imaged in the ALM during optical stimulation of the LC. The blue bar delineates the time during which stimulus pulses were given. Plots are mean and SEM. n = 103 trials in 3 mice representing 104 PVp and 69 PVn cells in 7 fields of view; rank-sum test comparing the means of the response prior to the tone and during the tone: PVp, p = 0.057; PVn, p = 0.39.

(D) Experimental mice; time series as (C). Note the increase in pupil diameter and PVp responses upon LC stimulation. n = 116 trials in 2 mice representing 86 PVp cells and 72 PVn cells imaged in 7 fields of view; rank-sum test comparing the means of the response prior to the tone and during the tone: PVp, p = 2.3e−18; PVn, p = 0.24.

at tone onset (Figures 4B and 4C). Similarly, PV cells from both functional groups were unaffected by tone presentation prior to conditioning (lighter shades in Figures 4E and 4F). Following fear conditioning, mice exhibited classic fear responses, although with a bit of a twist. When tone onset was immediately followed by pupil dilation, the onset of motor freezing began a few seconds later (Figure 4D). Head-fixed on the floating polystyrene spherical treadmill, mice could not immediately stabilize this treadmill and freeze. Executing this took roughly 5–6 s, during which the measurements of spherical treadmill motion clearly reflected the effort to stabilize and freeze. Somewhat serendipitously, this mismatch in pupil and motor responses proved valuable to the interpretation of the PV cell response data.

At tone onset, the responses of PVp cells increased in lockstep with pupil diameter, and these two measures remained high for the duration of the tone (Figures 4E and 4G). The responses of PVn cells, by contrast, were not noticeably altered until motor movement ceased. When motor freezing was evident, the responses of PVn cells climbed, presumably because the cholinergic suppression of these cells that accompanies motor movement was now relieved (Figures 4F and 4H). Of added interest, it seems that, during the period of complete freezing, the activities of both the PVp and PVn groups were elevated, indicating that these two groups do not strongly inhibit one another. These behavioral measures support the view that PVp and PVn cells establish functional subnetworks that can be differentially engaged.

DISCUSSION

These data indicate that PV cells establish stable and functionally distinct subnetworks in the neocortex and that the responses of these networks are independently modulated by separate components of the ascending reticular activating system, with one group suppressed when acetylcholine is released from basal forebrain cortical projections during locomotion and the other enhanced by norepinephrine release from the LC during periods of heightened arousal. We examined only two external correlates of PV cell responses, running speed and pupil diameter, and found two functional subnetworks. It is very much a possibility that if we had been able to measure some additional external behaviors, then PV cell responses could be further subdivided and that these functional divisions would also be stable over weeks and, perhaps, the lifetime of the animal. Should this be the case, it would indicate that PV cells exist in something akin to a Venn diagram, in which some cells could be involved in more than one behavior while still existing in a stable subnetwork.

We also note that we do not know where acetylcholine and norepinephrine are exerting their influence on PV cells. The cholinergic suppression of one group of PV cells suggests the engagement of an inhibitory-inhibitory circuit, such as the well-characterized vasoactive intestinal peptide (VIP) cell-mediated inhibition of PV cells (Lagler et al., 2016; Pi et al., 2013; Pfeffer et al., 2013). VIP cells are directly excited by acetylcholine, and, during some behaviors, this VIP cell inhibition of PV cells is engaged. This suppression may also be direct via the actions of acetylcholine on PV cells (Alitto and Dan, 2013). The excitatory effects of norepinephrine on the other group of PV cells may be direct or enhanced by local excitatory neuron input to PV cells.

Last, a transcriptome analysis of inhibitory cell types in the ALM found only one group of PV cells in layer 2/3 (Tasic et al., 2017). Our data indicate that such genetic clustering does not reveal the distinctions in their functional engagement.

How, precisely, neuromodulators act on inhibitory circuitry is incompletely understood. Given the effect of neuromodulation and inhibition on shaping the cortical state during development, attention, and learning and its loss during aging, understanding this microcircuitry of brain state is paramount. The data presented here, which establish the presence of functional subnetworks of PV cells, add nuance to the view that inhibitory neurons regulate the cortical state in a task-specific manner (Kvitsiani et al., 2013; Pinto and Dan, 2015; Kepecs and Fishell, 2014; Tovote et al., 2015). The state-dependent engagement of specific PV cell subnetworks would almost certainly influence the emergence of behavior-specific network responses (Dembrow and Johnston, 2014; Musall et al., 2018).

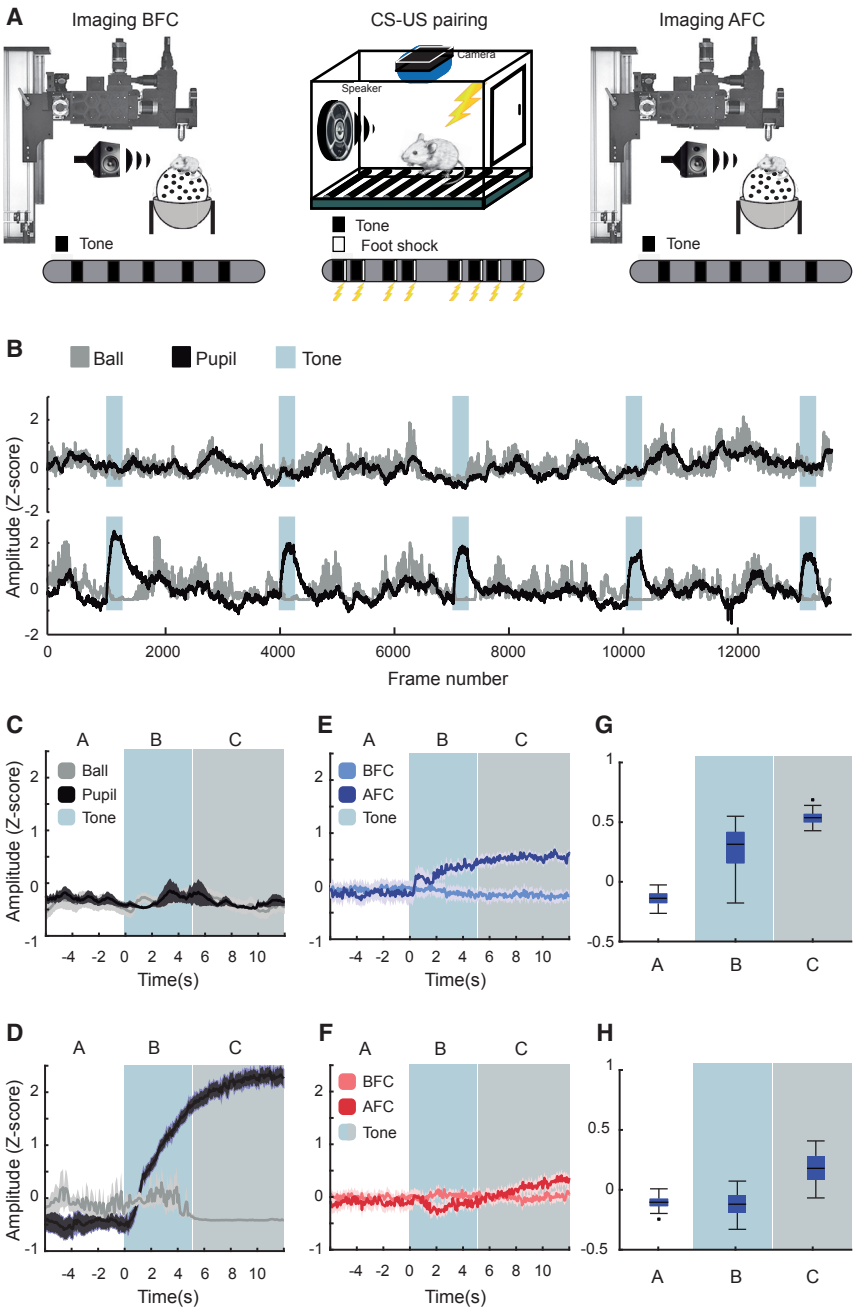

Figure 4. Responses of PVp and PVn Cells during Associative Fear

(A) Schematic of the imaging and training approach. Pupil diameter, running speed, and GCaMP6s responses in PV cells were imaged as head-fixed mice were exposed to five 2-kHz tones. Mice were then exposed to five 2-kHz tones that were each paired with a foot shock in a standard training cage. The following day, GCaMP6s responses of the same PV cells were imaged, and again the mouse was exposed to five 2-kHz tones.

(B) Plots of running speed (gray) and pupil diameter (black) for the same 7 mice before (top) and after (bottom) association of the tone with a foot shock. In both plots, the presentation of the tone is defined by the blue-gray rectangles. Note the large increase in pupil diameter and cessation of running during each tone after the association was learned. The PV cells imaged and analyzed in the remaining panels were derived from these 7 mice.

(C) Plot of mean and SD of running speed and pupil diameter to 2-kHz tone presentations prior to fear conditioning. The white background indicates time prior to tone presentation in seconds. The blue background highlights responses during the first 5 s after tone onset. The gray background identifies the remaining time during which the tone is present.

(D) The same plot as in (C) but after fear conditioning. Note that, although the pupil diameter increases at tone onset, running does not stop until about 5–6 s later (blue-to-gray transition).

(E) Plot of PVp responses to 2-kHz tones before (light blue) and after (dark blue) fear conditioning. 118 PVp cells were longitudinally imaged in 7 mice; 5 tone epochs per mouse.

(F) The same plot as in (E) but for PVn cells. 89 PVn cells were longitudinally imaged in the same regions of interest from the same 7 mice.

(G) Boxplots of PVp GCaMP6s fluorescence changes in units of *Z* score in the 6 s prior to (A), during the first 6 s after (B), and seconds 6–12 after (C) tone onset. These time bins were chosen because running stops approximately 6 s after tone onset. Note the immediate increase and continued increase in PVp responses after tone onset ($p = 0$, rank-sum test). The response continues to climb thereafter ($p = 3.55e{-}16$, rank-sum test);

(H) The same plot as in (G) but for PVn cells. Note that there is small but significant drop in GCaMP6s response distributions in the first 6 s after the tone, consistent with the increase in motor control to stabilize the ball ($p = 1.5e{-}7$, rank-sum test). When running stops and freezing begins (gray area), these responses increase significantly ($p = 4.4e{-}98$, rank-sum test).

STAR★METHODS

Detailed methods are provided in the online version of this paper and include the following:

- KEY RESOURCES TABLE
- CONTACT FOR REAGENT AND RESOURCE SHARING
- EXPERIMENTAL MODEL AND SUBJECT DETAILS
- METHOD DETAILS
  - Surgery, viral injection
  - Imaging
  - Pharmacology
  - Optogenetic stimulation of LC
  - Fear conditioning
- QUANTIFICATION AND STATISTICAL ANALYSIS
- DATA AND SOFTWARE AVAILABILITY

SUPPLEMENTAL INFORMATION

Supplemental Information includes two figures and can be found with this article online at https://doi.org/10.1016/j.celrep.2019.02.005.

ACKNOWLEDGMENTS

This work was supported by NIH R01 EY023871 (to J.T.T.) and NIH R01 EY018322 and EB022915 (to D.L.R.). P.G.-J.-C. was supported by postdoctoral contract from Junta de Andalucía (P12-CTS-2232) and by the Ramon y Cajal programme (RYC-2016-19906). We thank Luis de Lecea for the generous gift of the TH-Cre mice.

AUTHOR CONTRIBUTIONS

P.G.-J.-C. and J.T.T. conceived the study, analyzed the data, wrote the manuscript, and prepared the figures. P.G.-J.-C. collected the data presented in Figures 1, 2, 4, S1, and S2. E.T. collected the data presented in Figure 3. D.L.R. provided the MATLAB analysis code as well as all of the code for data acquisition via 2-photon microscopy.

DECLARATION OF INTERESTS

J.T.T. is a co-founder and co-owner of Neurolabware.

Received: September 10, 2018
Revised: December 6, 2018
Accepted: February 1, 2019
Published: February 26, 2019

REFERENCES

Alitto, H.J., and Dan, Y. (2013). Cell-type-specific modulation of neocortical activity by basal forebrain input. Front. Syst. Neurosci. *6*, 79.

Bennett, C., Arroyo, S., and Hestrin, S. (2014). Controlling brain states. Neuron *83*, 260–261.

Chen, T.W., Wardill, T.J., Sun, Y., Pulver, S.R., Renninger, S.L., Baohan, A., Schreiter, E.R., Kerr, R.A., Orger, M.B., Jayaraman, V., et al. (2013). Ultrasensitive fluorescent proteins for imaging neuronal activity. Nature *499*, 295–300.

Dembrow, N., and Johnston, D. (2014). Subcircuit-specific neuromodulation in the prefrontal cortex. Front. Neural Circuits *8*, 54.

Foote, S.L., Aston-Jones, G., and Bloom, F.E. (1980). Impulse activity of locus coeruleus neurons in awake rats and monkeys is a function of sensory stimulation and arousal. Proc. Natl. Acad. Sci. USA *77*, 3033–3037.

Guo, Z.V., Li, N., Huber, D., Ophir, E., Gutnisky, D., Ting, J.T., Feng, G., and Svoboda, K. (2014). Flow of cortical activity underlying a tactile decision in mice. Neuron *81*, 179–194.

Guo, Z.V., Inagaki, H.K., Daie, K., Druckmann, S., Gerfen, C.R., and Svoboda, K. (2017). Maintenance of persistent activity in a frontal thalamocortical loop. Nature *545*, 181–186.

Harris, K.D., and Thiele, A. (2011). Cortical state and attention. Nat. Rev. Neurosci. *12*, 509–523.

Hippenmeyer, S., Vrieseling, E., Sigrist, M., Portmann, T., Laengle, C., Ladle, D.R., and Arber, S. (2005). A developmental switch in the response of DRG neurons to ETS transcription factor signaling. PLoS Biol. *3*, e159.

Inagaki, H.K., Inagaki, M., Romani, S., and Svoboda, K. (2018). Low-Dimensional and Monotonic Preparatory Activity in Mouse Anterior Lateral Motor Cortex. J. Neurosci. *38*, 4163–4185.

Kepecs, A., and Fishell, G. (2014). Interneuron cell types are fit to function. Nature *505*, 318–326.

Kvitsiani, D., Ranade, S., Hangya, B., Taniguchi, H., Huang, J.Z., and Kepecs, A. (2013). Distinct behavioural and network correlates of two interneuron types in prefrontal cortex. Nature *498*, 363–366.

Lagler, M., Ozdemir, A.T., Lagoun, S., Malagon-Vina, H., Borhegyi, Z., Hauer, R., Jelem, A., and Klausberger, T. (2016). Divisions of Identified Parvalbumin-Expressing Basket Cells during Working Memory-Guided Decision Making. Neuron *91*, 1390–1401.

Lee, S.H., Kwan, A.C., Zhang, S., Phoumthipphavong, V., Flannery, J.G., Masmanidis, S.C., Taniguchi, H., Huang, Z.J., Zhang, F., Boyden, E.S., et al. (2012). Activation of specific interneurons improves V1 feature selectivity and visual perception. Nature *488*, 379–383.

Lee, A.M., Hoy, J.L., Bonci, A., Wilbrecht, L., Stryker, M.P., and Niell, C.M. (2014). Identification of a brainstem circuit regulating visual cortical state in parallel with locomotion. Neuron *83*, 455–466.

Madisen, L., Zwingman, T.A., Sunkin, S.M., Oh, S.W., Zariwala, H.A., Gu, H., Ng, L.L., Palmiter, R.D., Hawrylycz, M.J., Jones, A.R., et al. (2010). A robust and high-throughput Cre reporting and characterization system for the whole mouse brain. Nat. Neurosci. *13*, 133–140.

McGinley, M.J., David, S.V., and McCormick, D.A. (2015). Cortical Membrane Potential Signature of Optimal States for Sensory Signal Detection. Neuron *87*, 179–192.

Mineault, P.J., Tring, E., Trachtenberg, J.T., and Ringach, D.L. (2016). Enhanced Spatial Resolution During Locomotion and Heightened Attention in Mouse Primary Visual Cortex. J. Neurosci. *36*, 6382–6392.

Musall, S., Kaufman, M.T., Gluf, S., and Churchland, A.K. (2018). Movement-related activity dominates cortex during sensory-guided decision making. bioRxiv. https://doi.org/10.1101/308288.

Pfeffer, C.K., Xue, M., He, M., Huang, Z.J., and Scanziani, M. (2013). Inhibition of inhibition in visual cortex: the logic of connections between molecularly distinct interneurons. Nat. Neurosci. *16*, 1068–1076.

Pi, H.J., Hangya, B., Kvitsiani, D., Sanders, J.I., Huang, Z.J., and Kepecs, A. (2013). Cortical interneurons that specialize in disinhibitory control. Nature *503*, 521–524.

Pinto, L., and Dan, Y. (2015). Cell-Type-Specific Activity in Prefrontal Cortex during Goal-Directed Behavior. Neuron *87*, 437–450.

Polack, P.O., Friedman, J., and Golshani, P. (2013). Cellular mechanisms of brain state-dependent gain modulation in visual cortex. Nat. Neurosci. *16*, 1331–1339.

Reimer, J., Froudarakis, E., Cadwell, C.R., Yatsenko, D., Denfield, G.H., and Tolias, A.S. (2014). Pupil fluctuations track fast switching of cortical states during quiet wakefulness. Neuron *84*, 355–362.

Reimer, J., McGinley, M.J., Liu, Y., Rodenkirch, C., Wang, Q., McCormick, D.A., and Tolias, A.S. (2016). Pupil fluctuations track rapid changes in adrenergic and cholinergic activity in cortex. Nat. Commun. *7*, 13289.

Stringer, C., Pachitariu, M., Steinmetz, N.A., Reddy, C.B., Carandini, M., and Harris, K.D. (2018). Spontaneous behaviors drive multidimensional, brain-wide population activity. bioRxiv. https://doi.org/10.1101/306019.

Tasic, B., Yao, Z., Smith, K.A., Graybuck, L., Nguyen, T.N., Bertagnolli, D., Goldy, J., Garren, E., Economo, M.N., Viswanathan, S., et al. (2017). Shared and distinct transcriptomic cell types across neocortical areas. bioRxiv. https://doi.org/10.1101/229542.

Tovote, P., Fadok, J.P., and Lüthi, A. (2015). Neuronal circuits for fear and anxiety. Nat. Rev. Neurosci. *16*, 317–331.

Vinck, M., Batista-Brito, R., Knoblich, U., and Cardin, J.A. (2015). Arousal and locomotion make distinct contributions to cortical activity patterns and visual encoding. Neuron *86*, 740–754.

Wilson, N.R., Runyan, C.A., Wang, F.L., and Sur, M. (2012). Division and subtraction by distinct cortical inhibitory networks in vivo. Nature *488*, 343–348.

STAR★METHODS

KEY RESOURCES TABLE

REAGENT or RESOURCE	SOURCE	IDENTIFIER
Bacterial and Virus Strains		
AAV1.Syn.Flex.GCaMP6s.WPRE.SV40	Addgene/Penn Vector Core Transfer	Addgene ID: 100845-AAV1
AAV-flex-rev-ChR2-tdTomato	addgene/Penn Vector Core Transfer	Addgene ID 18917-AAV1
Chemicals, Peptides, and Recombinant Proteins		
Mecamylamine	Sigma	Cat#M9020
Propranolol	Sigma	Cat#P0884
Prazosin	Sigma	Cat#P7791
Yohimbine	Sigma	Cat#Y3125
Experimental Models: Organisms/Strains		
Mouse: PV^{Cre}: B6;129P2-$Pvalb^{tm1(cre)Arbr}$/J	JAX	Stock No: 008069
Mouse: Ai9: B6.Cg-Gt(ROSA)26$Sor^{tm9(CAG-tdTomato)Hze}$/J	JAX	Stock No: 007905
Mouse: Th-IRES-Cre: B6;129X1-$Th^{tm1(cre)Te}$/Kieg	European Mouse Mutant Archive	EMMA ID: EM:00254
Software and Algorithms		
Custom MATLAB scripts	Mathworks	https://www.mathworks.com

CONTACT FOR REAGENT AND RESOURCE SHARING

Further information and requests for resources and reagents should be directed to and will be fulfilled by the Lead Contact, Pablo Garcia-Junco-Clemente (pgarciajunco@gmail.com).

EXPERIMENTAL MODEL AND SUBJECT DETAILS

All procedures were approved by UCLA's Office of Animal Research Oversight (the Institutional Animal Care and Use Committee, IACUC) and were in accord with guidelines set by the US National Institutes of Health. A total of 33 mice, both male (10) and female (23), aged P45-56, were used for *in vivo* imaging. PV-Cre lines were obtained from the Jackson Laboratory (JAX Stock#: 008069) and crossed with Ai9 mice (B6;129S6-*Gt(ROSA)26Sor*$^{tm9(CAG-tdTomato)Hze}$/J; JAX Stock#: 007905), to express td-Tomato in a CRE-dependent manner. Tyrosine hydroxylase-Cre (a generous gift from Luis de Lecea at Stanford University; which can also be obtained directly from the European Mouse Mutant Arcive Th-IRES-Cre: B6;129X1-$Th^{tm1(cre)Te}$/Kieg; EM:00254) were also crossed with PV-Cre lines. All mouse lines were crossed into a C57 black 6 background for 7 generations or longer. Mice were housed in groups of 2-3 per cage in a normal 12/12 light dark cycle. Animals were naive subjects with no prior history of participation in research studies.

METHOD DETAILS

Surgery, viral injection

Craniotomy survival surgery, virus injection (AAV1.Syn.Flex.GCaMP6s.WPRE.SV40: Addgene ID: 100845-AAV1), GCaMP6s imaging, motion correction, and cell segmentation were as reported in reference (Mineault et al., 2016). The coordinates used for these studies in ALM were 2.8mm anterior to Bregma and 1.5mm lateral of the sagittal suture. For the experiments in primary visual cortex, the coordinates used were 1mm anterior of Lambda and 3mm lateral of the sagittal suture.

Imaging

Once expression of GCaMP6 was observed, typically between 12-15 days after the injection, imaging sessions took place. Imaging was performed using a resonant scanning, two-photon microscope (Neurolabware, Los Angeles, CA) controlled by Scanbox acquisition software (Scanbox, Los Angeles, CA). The light source was a Coherent Chameleon Ultra II laser (Coherent Inc, Santa Clara, CA) running at 920nm. The objective was an x16 water immersion lens (Nikon, 0.8NA, 3mm working distance). The microscope frame rate was 15.5Hz (512 lines with a resonant mirror at 8kHz). Eye movements and pupil size were recorded via a Dalsa Genie M1280 camera (Teledyne Dalsa, Ontario, Canada) fitted with a 740nm long-pass filter. Images were captured at an average depth of 210 μm (90% of

imaging fields within the range 125-300 microns). During imaging a substantial amount of light exits from the brain through the pupil. Thus, no additional illumination was required to image the pupil. Mice were head-fixed on a floating, spherical treadmill on which they had been trained to balance and run. All mice were trained on the spherical treadmill for 3 days, 20-minutes per day before experiments were started. Movement of the spherical treadmill was recorded via a Dalsa Genie M640 camera. Both locomotion and eye movement data were synchronized to the microscope frames. We first summed images over a 30 s. period to obtain a high signal-to-noise image of Cre-dependent tdTomato expression, using 1000nm excitation, to identify PV cells. We then changed the wavelength to 920nm and imaged GCaMP6(f/s) dynamics during 10-15 minutes per field. Mice were head fixed, but freely moving during the entire imaging session.

Pharmacology

The cholinergic, noradrenergic and glutamatergic Mecamylamine M9020, Yohimbine Y3125, Propranolol P0884, Prazosin P7791, and atropine were purchased from Sigma. Drugs were dissolved in warm cortex buffer and filtered and then injected into cortex using a glass micropipette using a picospritzer. During the initial surgery and AAV injection, a hole was drilled through each coverslip which was ultimately used to form the cranial window. This hole was plugged using kwik-sil and covered with acrylic to prevent desiccation and infection. During imaging, 2 weeks after AAV injection, the kwik-sil was removed, GCaMP6-expressing neurons were imaged for 15 minutes, and then the mouse was removed from the microscope and placed under a dissection microscope. The glass micropipette containing the filtered drugs was then inserted into the cortex via the previously-drilled hole. This permitted the maintenance of the cranial window intact. The mouse was then placed back under the 2-photon microscope, the same neurons were again found, and their activities imaged for another 15 minutes.

Optogenetic stimulation of LC

Offspring from crosses of Tyrosine hydroxylase-Cre (a generous gift from Luis de Lecea at Stanford University; can also be obtained directly from the European Mouse Mutant Arcive Th-IRES-Cre: B6;129X1-$Th^{tm1(cre)Te}$/Kieg; EM:00254) and PV-Cre mice were used. AAV-flex-rev-ChR2-tdTomato (Addgene ID 18917-AAV1, titer: 20-30 nL at $\sim 10^{12}$ genome copies per mL) was pressure injected into locus coeruleus (AP -5.45mm, ML 1.28mm, DV 3.65mm) using a glass micropipette. Immediately thereafter, a fiber optic cannula (Prizmatix Ltd; 2.5mm ferrule, 200um diameter fiber) was implanted at an angle of 15 degrees to target LC in order to provide access for future placement of the imaging objective lens. The cannula was cemented to the skull using dental acrylic. Next, a craniotomy was performed over ALM as above and AAV-flex-GCaMP6s was pressure injected as above and a head bar cemented to the skull. Two weeks later, PV cells were imaged as above. During this time, 18-20 epochs of light trains were delivered to LC using a high-power density 460nm blue LED (Prizmatix) only during periods of behavioral quiescence when the pupil was constricted. Stimuli consisted to 40 10ms duration trains delivered at 15.5Hz synchronized to acquisition frame rate. Only epochs in which pupil dilation was phase-locked to LC stimulation were analyzed in experimental animals. Mice were then transcardially perfused and brains sectioned to verify expression of tdTomato in locus coeruleus.

Fear conditioning

Responses of PV cells in ALM, as well as any changes in running and pupil dilation to presentation of 2KHz tones were first measured prior to fear conditioning by exposing mice to the 2KHz tones while head-fixed under the 2-photon microscope. For fear conditioning, these same mice were then conditioned to associate a 2KHz tone with a mild foot shock by placing them in a rectangular chamber with a base composed of evenly spaced metal bars. In this chamber, mice received eight randomly delivered 2KHz tone presentations during a single training that lasted 15min. Each tone epoch lasted 15 s. During the final second, a 0.65mA shock was delivered to the mouse's feet via metal bars on the bottom of the chamber. Responses of the same PV cells in these same mice, changes in locomotion and pupil diameter after fear association were then measured by exposing the mice to the tones while head-fixed under the 2-photon microscope, fear was measured behaviorally by a large increase in pupil dilation as well as a cessation of running. In this context, the first tone was delivered 1 minute after imaging started, and the subsequent 4 tones were given every 3 minutes thereafter (duration = 15sec, 2KHz tone).

QUANTIFICATION AND STATISTICAL ANALYSIS

Data collection and analysis was not blinded. No randomization was used to assign subject to the experimental groups. Experiments required mice of known genotype, making randomization impossible. Statistical tests, numbers of mice, fields of view, numbers of cells, and P values are reported in each figure legend.

All statistical analyses were done using non-parametric procedures in MATLAB. Significance levels were set to $\alpha < 0.05$ for all two-group comparisons. Mann-Whitney U tests were employed for testing differences between independent groups, while groups with repeated-measures were compared with the Wilcoxon signed-rank test. In comparisons involving more than two groups, custom written MATLAB code was used to tailor an ANOVA to non-normally distributed data with unequal variances, for independent and non-independent groupings: F-statistics were computed as the ratio between sum of squares among groups and sum of squares within groups, and p values were calculated by comparing the F-statistic derived from the data and the average F-statistic generated from resampling the shuffled data 10,000 times. Our data required 2 types of ANOVAs: 2-way ANOVA with repeated-measures and

one-way ANOVA with repeated-measures (Kruskal-Wallis test). ANOVAs were followed by post hoc comparisons. The Bonferroni method was used to correct for multiple comparisons.

DATA AND SOFTWARE AVAILABILITY

Custom code will be provided upon request to J.T.T. The purpose of the custom scripts was to read in the acquired fluorescence, pupil diameter, and locomotion time series; to evaluate the significance of correlations between them; to examine clustering of the signals; to examine changes in fluorescence relative to the timing of optogenetic stimulation; to perform statistical analyses; and to plot these data.

Cell Reports, Volume *26*

Supplemental Information

State-Dependent Subnetworks of Parvalbumin-Expressing Interneurons in Neocortex

Pablo Garcia-Junco-Clemente, Elaine Tring, Dario L. Ringach, and Joshua T. Trachtenberg

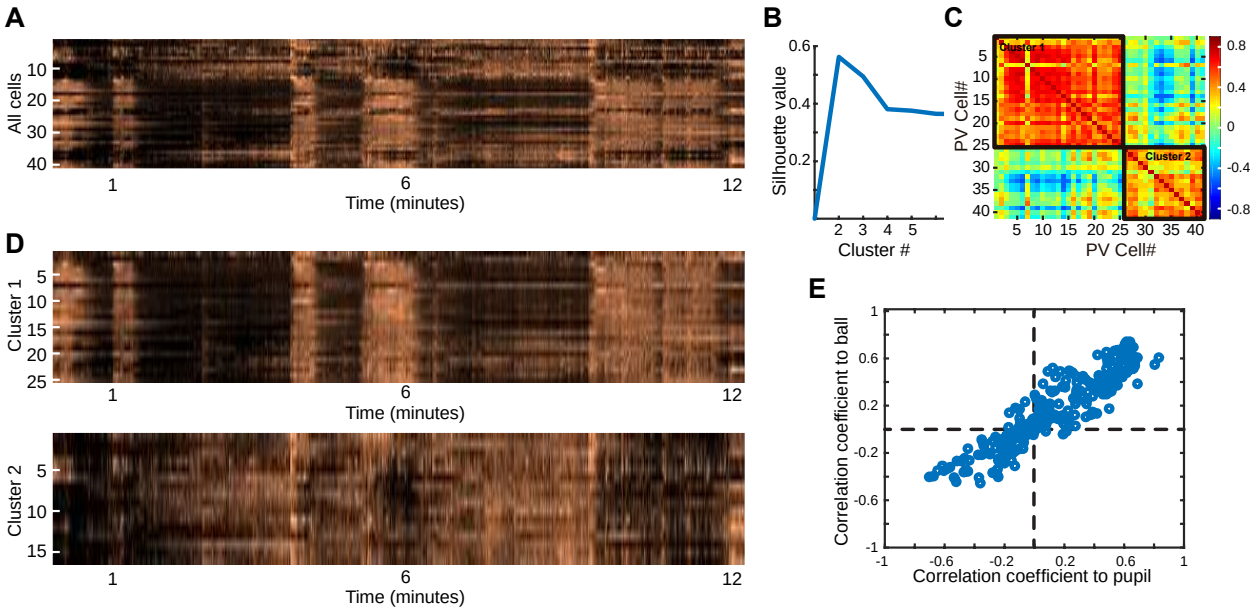

Figure S1. Two functional groups of PV cells in primary visual cortex. Related to Figure 1

A. An example of GCaMP6s fluorescent changes imaged across 41 PV cells in primary visual cortex over 12 minutes in an alert, head-fixed mouse. Color map as in Figure 1.

B. Plot of silhouette value versus cluster number following k-means cluster analysis, identifying 2 major functional clusters of PV cells.

C. Plot of correlation coefficient of the activity of each cell in panel (A) to all other cells. Note the emergence of two groups, labeled Cluster 1 and Cluster 2.

D. Time series of GCaMP6 responses for cells in Cluster 1 in panel C (top), and Cluster 2 in panel C (bottom). Note the negative correlation in the responses of these two groups.

E. Plot of each cell's correlation coefficient to pupil diameter (abscissa) and to locomotion (ordinate). 6 mice, 6 fields of view, 289 PV cells (195 PVp, 94 PVn).

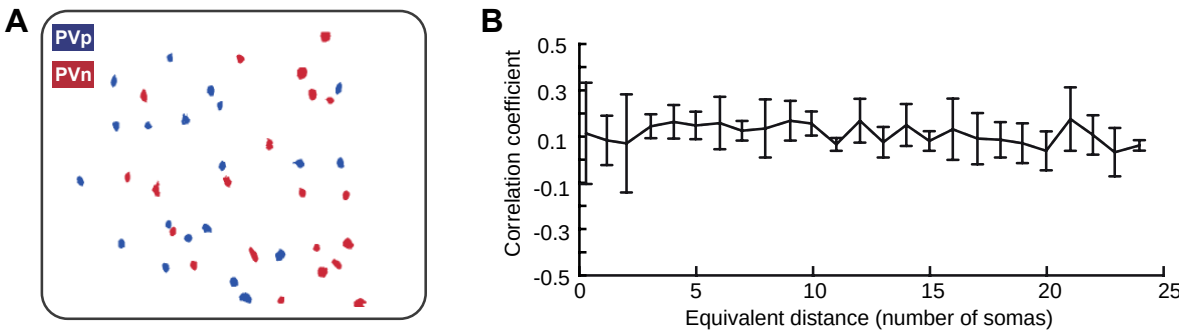

Figure S2. PVp and PVn cells are are not spatially clustered. Related to Figure 1

A. Example of the relative positions of 21 PVn and 20 PVp cells in a single field of view. Image is 800um by 500um.

B. Mean and standard deviation of the correlation coefficients of responses for all PV cells imaged in ALM across all mice plotted as a function of distance. Note the absence of slope in this plot. 11 mice, 21 fields of view, 747 PV cells (344 PVp, 403 PVn).